Magnetoelectric effect and spontaneous polarization in HoFe$_3$(BO$_3$)$_4$ and Ho$_{0.5}$Nd$_{0.5}$Fe$_3$(BO$_3$)$_4$

R. P. Chaudhury,[1] F. Yen,[2] B. Lorenz,[1] Y. Y. Sun,[1] L. N. Bezmaternykh,[3] V. L. Temerov,[3] and C. W. Chu[1,4,5]

[1]*TCSUH and Department of Physics, University of Houston, Houston, Texas 77204-5002, USA*

[2]*Applied Superconductivity Laboratory, Southwest Jiaotong University, Chengdu, Sichuan 610031, China*

[3]*Institute of Physics, Siberian Division, Russian Academy of Sciences, Krasnoyarsk 660036, Russia*

[4]*Lawrence Berkeley National Laboratory, 1 Cyclotron Road, Berkeley, California 94720, USA*

[5]*Hong Kong University of Science and Technology, Hong Kong, China*

The thermodynamic, magnetic, dielectric, and magnetoelectric properties of HoFe$_3$(BO$_3$)$_4$ and Ho$_{0.5}$Nd$_{0.5}$Fe$_3$(BO$_3$)$_4$ are investigated. Both compounds show a second order Néel transition above 30 K and a first-order spin reorientation transition below 10 K. HoFe$_3$(BO$_3$)$_4$ develops a spontaneous electrical polarization below the Néel temperature (T_N) which is diminished in external magnetic fields. No magnetic-field induced increase of the polarization could be observed in HoFe$_3$(BO$_3$)$_4$. In contrast, the solid solution Ho$_{0.5}$Nd$_{0.5}$Fe$_3$(BO$_3$)$_4$ exhibits both, a spontaneous polarization below T_N and a positive magnetoelectric effect at higher fields that extends to high temperatures. The superposition of spontaneous polarization, induced by the internal magnetic field in the ordered state, and the magnetoelectric polarizations due to the external field results in a complex behavior of the total polarization measured as a function of temperature and field.

I. INTRODUCTION

The rare earth iron borates, RFe$_3$(BO$_3$)$_4$ (R=rare earth, Y), belong to the trigonal system with space group R32.[1] Their structure is similar to that of the mineral CaMg$_3$(CO$_3$)$_4$ (huntite), a trigonal trapezohedral structure that is one of the five trigonal types. This class of compounds has attracted recent attention because of a large magnetoelectric effect observed in GdFe$_3$(BO$_3$)$_4$ (Refs. 2–5) and in NdFe$_3$(BO$_3$)$_4$.[6] The noncentrosymmetric structure makes these materials also an interesting candidate for optical applications based on their good luminescent and nonlinear optical properties.[7–9] Thermodynamic and magnetic measurements have indicated a wealth of structural and magnetic phase transitions with ordering of Fe-spins as well as the rare earth moments involved. The majority of the RFe$_3$(BO$_3$)$_4$ compounds exhibit a structural phase transition from the high-temperature structure with R32 space group (No. 155) to the low-temperature P3$_1$21 structure (No. 152).[10–12] The structure change is accompanied by a distinct anomaly of the heat capacity.[12,13] The R32↔P3$_1$21 transition temperature, T_S, scales with the ionic radius of the rare earth and for some (R=Ho, Dy and Y) this transition takes place above room temperature. Other physical quantities, for example the dielectric constant, exhibit distinct and sharp anomalies at T_S.[5,11]

Magnetic measurements at high-temperature reveal a strong antiferromagnetic (AFM) correlation between the Fe spins resulting in an AFM transition at the Néel temperature, T_N, into the AFM2 phase below 40 K.[12] Again, T_N scales with the rare earth element decreasing from 40 K (Ho) to 22 K (La). Below T_N, the magnetic interaction of rare earth moments with the ordered Fe spins becomes stronger and results in a magnetic polarization of the rare earth system and, in some rare cases, in a spin reorientation transition into the AFM1 phase at lower temperatures that is driven by the magnetocrystalline anisotropy of the rare earth moment.

The spin reorientation transition was originally only observed in GdFe$_3$(BO$_3$)$_4$ at T_{SR}=9 K and its magnetic field-temperature (H-T) phase diagram was extensively studied.[5,14–16] However, recent neutron scattering experiments[17] have found evidence for a similar spin reorientation in HoFe$_3$(BO$_3$)$_4$ at a slightly lower temperature of 5 K. The peculiarities of the crystallographic structure, the various possibilities for the Fe spins to interact via direct or superexchange, and the coupling with the rare earth moments result in complex magnetic structures and the cascade of phase transitions upon decreasing temperature, as observed in GdFe$_3$(BO$_3$)$_4$.[15] The magnetic structure has been resolved for only a few rare earth iron borates through magnetic x-ray scattering (R=Gd) (Ref. 18) and neutron scattering (R=Nd, Tb, and Ho) experiments.[17,19,20]

Since the discovery of a large magnetoelectric effect in gadolinium iron borate,[2] the control of the electrical polarization through magnetic fields in GdFe$_3$(BO$_3$)$_4$ has become the focus of interest. The complex magnetoelectric H-T phase diagram was studied through polarization, dielectric constant, magnetic, and heat capacity measurements.[2–5,14,16,21] The combination of polarization and magnetostriction experiments have proven the intimate correlation of the magnetoelastic and magnetoelectric properties of the compound.[2,3,22] The sharp and sizable increase of the electrical polarization and the magnetostriction effect is mainly observed at the spin reorientation phase transition between the AFM2 and AFM1 phases. The field-induced polarization (FIP) phase is well resolved in a plateaulike structure of the dielectric constant $\varepsilon(T)$ and the complete H-T phase diagram was resolved for different orientations of the external field H.[5] The magnetoelectric and magnetoelastic properties of GdFe$_3$(BO$_3$)$_4$ have been qualitatively described by a model taking into account the symmetry of the system and the lowest order expansion of the thermodynamic potential with respect to the magnetic exchange.[22]

The search for other rare earth iron borates with a significant magnetoelectric effect has been successful and

$NdFe_3(BO_3)_4$ was discovered as the second candidate showing a large field-induced polarization.[6,21] Contrary to $GdFe_3(BO_3)_4$ no spin reorientation transition could be detected in $NdFe_3(BO_3)_4$ through magnetization, thermodynamic, and neutron scattering experiments.[19,23,24] A small maximum of the magnetic susceptibility, observed at 6 K, was attributed to three-dimensional AFM order of the Fe^{3+} and Nd^{3+} sublattices.[25] It is remarkable that the magnetic-field-induced polarization in $NdFe_3(BO_3)_4$ exceeds the value in $GdFe_3(BO_3)_4$ by nearly two orders of magnitude. The sizable magnetoelectric coupling found in $GdFe_3(BO_3)_4$ and $NdFe_3(BO_3)_4$ is the motivation for the search for magnetoelectric effects in other rare earth iron borates. Ho is an interesting candidate because of a relatively large magnetic moment of the rare earth ion. Strong interactions with the Fe-spins and possible magnetoelectric effects are therefore expected in $HoFe_3(BO_3)_4$. In fact, the magnetic order in $HoFe_3(BO_3)_4$ below T_N was recently explored and it was shown to involve long range order of both, Fe spins and Ho moments.[17] At lower temperatures, $HoFe_3(BO_3)_4$ exhibits a spin reorientation similar to the one observed in $GdFe_3(BO_3)_4$. However, investigations of the dielectric and magnetoelectric properties have not been reported yet.

We have therefore synthesized large single crystals of $HoFe_3(BO_3)_4$ and of the solid solution $Nd_{0.5}Ho_{0.5}Fe_3(BO_3)_4$ and investigated their thermodynamic, magnetic, and magnetoelectric properties. We find that, even without external magnetic field, $HoFe_3(BO_3)_4$ exhibits an electric polarization below T_N which increases with decreasing temperature and suddenly drops to zero at the spin reorientation transition. The magnetic-field effect on the polarization and the $H\text{-}T$ phase diagram is investigated. $Nd_{0.5}Ho_{0.5}Fe_3(BO_3)_4$ shows a similar polarization effect upon decreasing temperature with an even higher value of the polarization as compared to $HoFe_3(BO_3)_4$. In addition, $Nd_{0.5}Ho_{0.5}Fe_3(BO_3)_4$ also exhibits a large magnetoelectric effect in external fields along the a axis with high values of the induced polarization.

The paper is organized as follows: Sec. II provides the essential information about sample synthesis and experimental equipment used for various measurements. The results are presented in Sec. III starting with data for $HoFe_3(BO_3)_4$ (magnetic, thermodynamic, and dielectric data) and followed by corresponding data for $Nd_{0.5}Ho_{0.5}Fe_3(BO_3)_4$. Section IV summarizes the main results and conclusions.

II. EXPERIMENTAL

Single crystals of $HoFe_3(BO_3)_4$ and $Nd_{0.5}Ho_{0.5}Fe_3(BO_3)_4$ were grown using $Bi_2Mo_3O_{12}$ based flux as described earlier.[26] The crystals were cut in different sizes and shapes to fit the demands of the various measurements. The orientation was determined by single crystal Laue x-ray diffractometry. For dielectric and polarization measurements thin plates (0.5 to 1 mm thick) were prepared and electrical contacts were attached to two parallel faces using silver paint. For dielectric constant measurements the high-precision capacitance bridge AH2500A (Andeen-Hagerling) was employed. The electrical polarization was extracted by integrating the pyroelectric current measured by the K6517A
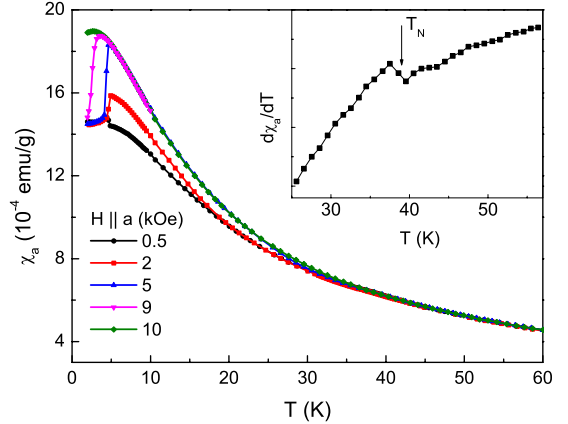

FIG. 1. (Color online) Magnetic susceptibility of $HoFe_3(BO_3)_4$ with the field oriented along the a axis. The inset shows the derivative, $d\chi_a/dT$, with the distinct anomaly at T_N.

electrometer (Keithley) upon variation of temperature or magnetic field. Temperature and field control were provided by the Physical Property Measurement System (PPMS, Quantum Design). The PPMS was also employed for heat capacity experiments. The magnetization was measured in a commercial superconducting quantum interference device (SQUID) magnetometer (MPMS, Quantum Design). Thermal expansion measurements were conducted using a home made high-precision capacitance dilatometer.[27]

III. RESULTS AND DISCUSSION

A. Magnetic phase diagram of $HoFe_3(BO_3)_4$

Early investigations have shown that the structural transition from R32 to P$3_1$21 in $HoFe_3(BO_3)_4$ happens well above room temperature. The critical temperatures, $T_S \simeq 420$ K and $T_N \simeq 39$ K, are among the highest of all rare earth iron borates.[12] The high magnetic ordering temperature and the easy-plane character of the Fe^{3+} spin alignment was revealed also in optical measurements using Er^{3+} ions as a spectroscopic probe.[28] The existence of a spin reorientation transition ($T_{SR} \simeq 5$ K) in $HoFe_3(BO_3)_4$, however, was detected only recently in neutron diffraction experiments at zero magnetic field.[17]

The magnetic susceptibilities of $HoFe_3(BO_3)_4$, measured perpendicular (χ_a) and parallel (χ_c) to the c axis, clearly reveal the distinct anomalies at both magnetic transition temperatures (Figs. 1 and 2). The Neél transition at $T_N = 38.5$ K is reflected in a minute change of slope of the a-axis susceptibility which is clearly visible in the derivative, $d\chi_a/dT$ (inset in Fig. 1). Below T_N the susceptibility shows a distinct dependence on the a-axis field, H_a. χ_a increases with H_a below 5 kOe (Fig. 1). This behavior is similar to the T dependence of χ_a of $GdFe_3(BO_3)_4$ which was interpreted as an effect of the in-plane ordering of the Fe spins leading to a reduction of χ_a between the Neél and spin reorientation temperatures at zero field.[5] At lower temperature, the spin reorientation transition is marked by a sharp step of χ_a. This step is positive with decreasing T for low magnetic fields $H_a < 1.2$ kOe, however, it turns negative for H_a between
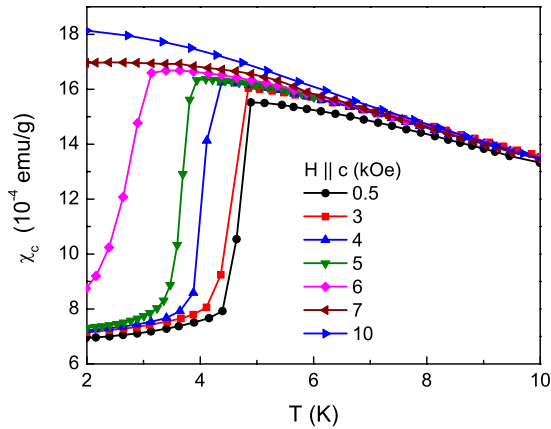
FIG. 2. (Color online) Low-temperature magnetic susceptibility of $HoFe_3(BO_3)_4$ with the field oriented along the c axis.

1.2 and 9 kOe. The sign change of this steplike anomaly is related to the magnetic order induced small decrease of χ_a in the AFM2 phase since χ_a is independent of the magnetic field in the AFM1 phase (Fig. 1). The decrease of χ_a at T_{SR} is different from the corresponding increase observed in $GdFe_3(BO_3)_4$. The origin of this difference may lie in the distinct magnetic structures of both compounds. The order of the Fe spins is incommensurate with no long-range order of the Gd-moments above T_{SR} in $GdFe_3(BO_3)_4$ (Ref. 18) but it is commensurate with the onset of Ho-moment order at T_N in $HoFe_3(BO_3)_4$.[17] T_{SR} quickly shifts to lower temperatures with increasing magnetic field and the AFM1 phase is completely suppressed for $H_a > 10$ kOe. The derived phase boundary between the AFM2 and AFM1 phases is shown in Fig. 3 (bold symbols).

The c-axis susceptibility shows no detectable anomaly at T_N and very little field dependence in the AFM2 phase. At the spin reorientation transition χ_c suddenly drops by 60% (Fig. 2). The resulting phase boundary is displayed in Fig. 3 (open symbols). The large decrease of χ_c in the AFM1 phase reflects the increased correlation and stiffness of the Fe spins
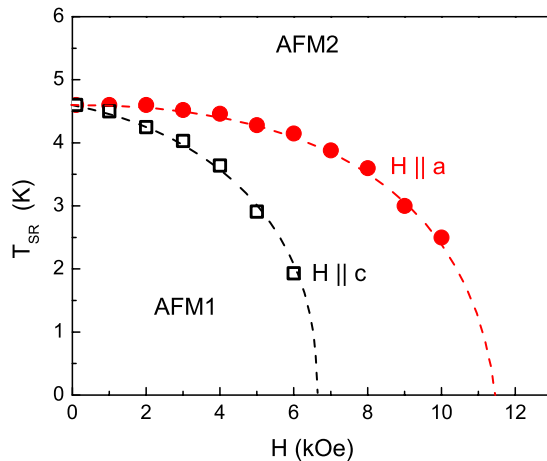

FIG. 3. (Color online) Low-temperature T-H phase diagram of $HoFe_3(BO_3)_4$ with the field aligned with the a axis (bold symbols) and the c axis (open symbols). The lines serve as a guide to the eyes.

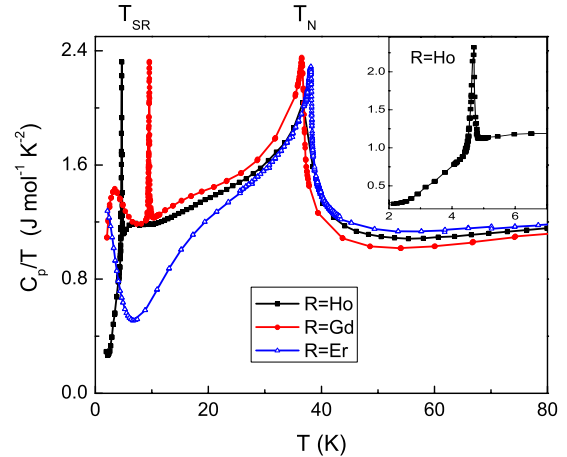FIG. 4. (Color online) Comparison of heat capacities of $HoFe_3(BO_3)_4$, $GdFe_3(BO_3)_4$, and $ErFe_3(BO_3)_4$. The inset shows the low-temperature heat capacity of $HoFe_3(BO_3)_4$ near T_{SR}.

after their rotation into a collinear spin structure oriented along the c axis that is induced by the strong coupling to the Ho moments with a large uniaxial magnetic anisotropy. The magnetic susceptibility data reveal a minute temperature hysteresis of about 0.1 K at T_{SR} indicating the first-order nature of the phase transition from the AFM2 to the AFM1 phase. The first-order nature of the spin reorientation phase transition was also suggested from the steplike change of the Ho and Fe moments derived from powder neutron scattering experiments.[17] The phase diagram is further explored by isothermal M-H measurements showing a metamagnetic transition (sudden increase of the magnetization $M(H)$ with field) at the spin reorientation transition. The critical fields are consistent with the phase boundaries of Fig. 3 derived from temperature dependent measurements. Similar to the $\chi(T)$ measurements the $M(H)$ data show a small field hysteresis across the AFM2→AFM1 phase boundary confirming the first order character of the transition.

The thermodynamic signature of the two magnetic phase transitions is revealed in heat capacity measurements. Figure 4 shows the heat capacity of $HoFe_3(BO_3)_4$ together with C_p of the related compounds $GdFe_3(BO_3)_4$ and $ErFe_3(BO_3)_4$ in a wide temperature range. The inset displays the low-temperature C_p of $HoFe_3(BO_3)_4$ near the spin reorientation transition on an expanded temperature scale. The Néel transition is characterized by a λ-shaped pronounced peak of $C_p(T)$ at 38.5 K suggesting the transition into the AFM2 phase to be a second order phase transition. This is consistent with the steady increase of the Fe sublattice magnetization below T_N observed in neutron scattering experiments.[17] However, the derived Fe magnetic moment does not follow closely the expected Brillouin function which was attributed to the coupling of the Fe spins with the Ho moments leading to a simultaneous order of both magnetic subsystems at T_N. The low-temperature peak of C_p at T_{SR} is extremely narrow as is expected at a first order transition. Below T_N, but above T_{SR}, C_p/T of $HoFe_3(BO_3)_4$ shows an enhancement with respect to similar data for other rare earth iron borates, e.g., $ErFe_3(BO_3)_4$ also shown in Fig. 4. This enhancement reflects the strong coupling between the rare earth moments and the
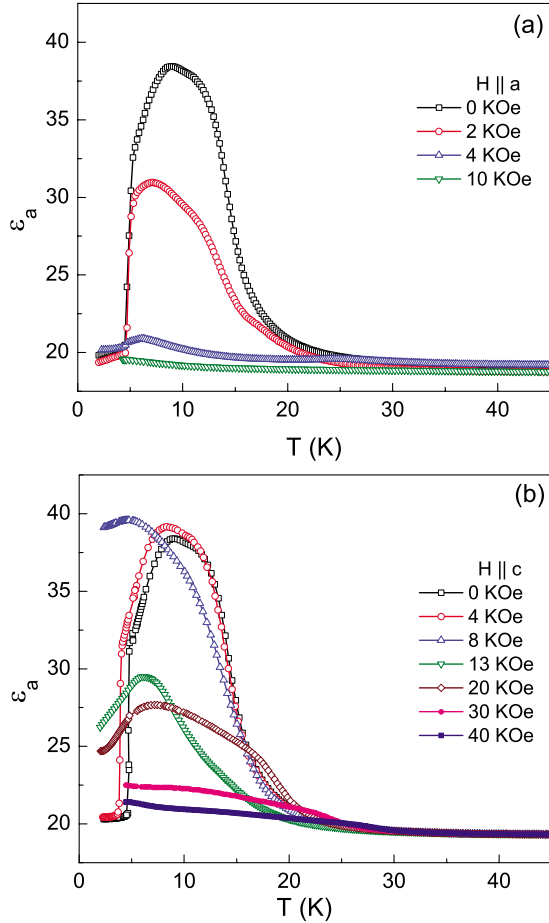
FIG. 5. (Color online) Dielectric constant, ε_a, of $HoFe_3(BO_3)_4$ at different magnetic fields $H\|a$ (a) and $H\|c$ (b).

Fe spin order resulting in the spin reorientation transition and the order of the rare earth moments. An equivalent enhancement of C_p/T was also observed in $GdFe_3(BO_3)_4$ (Fig. 4), the second $RFe_3(BO_3)_4$ with a spin reorientation transition.[5] The increased entropy associated with the enhanced heat capacity at low T was attributed to the eightfold degeneracy of the ground state level of the Gd^{3+} ion in the corresponding crystal field.[13] The heat capacity data for all three compounds are compared in Fig. 4. At the lowest temperatures a Schottky-type contribution to the heat capacity is most pronounced in $ErFe_3(BO_3)_4$ and $GdFe_3(BO_3)_4$, but barely visible in $HoFe_3(BO_3)_4$.

B. Magnetoelectric effect and polarization in $HoFe_3(BO_3)_4$

1. Dielectric constant in magnetic fields

Dielectric anomalies below the Neél transition have been observed in $GdFe_3(BO_3)_4$.[5] A small but distinct increase of the a-axis dielectric constant, ε_a, and its sudden drop at the spin reorientation transition was explained by the coupling of the magnetic order to the lattice. While the peaklike increase of ε_a in $GdFe_3(BO_3)_4$ is less than 1% of its value at T_N, the a-axis dielectric constant of $HoFe_3(BO_3)_4$ (Fig. 5) shows a colossal enhancement of nearly 100% below T_N. This huge increase from $\varepsilon_a=20$ to $\varepsilon_a=37$ indicates that the spin-lattice

coupling in $HoFe_3(BO_3)_4$ is two orders of magnitude stronger than the spin-lattice interaction in $GdFe_3(BO_3)_4$. With decreasing temperature ε_a passes through a maximum and drops suddenly back to its high-temperature value of 20 at the spin reorientation transition temperature, T_{SR}, as shown in Fig. 5.

The peak of ε_a is quickly suppressed by magnetic fields oriented along the a axis [Fig. 5(a)]. At 4 kOe, the peak height of ε_a has dropped by 90% and at 10 kOe it is completely absent. This extraordinary magnetodielectric effect shows the intricate correlation between the magnetic order and the dielectric properties of $HoFe_3(BO_3)_4$. With the magnetic field oriented along the c axis [Fig. 5(b)] the rise of ε_a below T_N persists to higher field values, up to $H_c\simeq 8$ kOe, beyond the critical field above which the spin reorientation transition is suppressed (see Fig. 3). The maximum $\varepsilon_a\simeq 40$ at 8 kOe is twice as large as its value near or above T_N. With further increasing field, however, the maximum of ε_a decreases quickly but a small enhancement below T_N is still detectable at c-axis fields as high as 40 kOe, as shown in Fig. 5(b). It is remarkable that the main increase of ε_a in the AFM2 phase happens well below the Neél temperature at about 20 K and that ε_a suddenly decreases at T_{SR} assuming a value in the AFM1 phase that is close to ε_a of the paramagnetic phase above T_N. This shows that the coupling between the magnetic order and the lattice is most significant in the AFM2 phase at zero magnetic field but it is negligibly small in the AFM1 phase. The c-axis dielectric constant, ε_c, was also measured and it shows a similar enhancement below T_N, however, the magnitude of the peak is much smaller and it amounts to only 3% of its base value.

A similar large magnetodielectric effect has been observed in some rare earth manganites, for example in orthorhombic $HoMnO_3$ below the Neél temperature.[29] It was later shown that the sharp increase of ε was associated with the development of a spontaneous electric polarization.[30] Therefore, we decided to search for pyroelectric and magnetoelectric effects below the Neél temperature of $HoFe_3(BO_3)_4$.

2. Polarization at zero magnetic field

The pyroelectric current measured between two parallel electrodes attached to a sample is proportional to the change of the sample's polarization due to a change of temperature or magnetic field. In general, a bias voltage can be applied during the measurement or it can be used to align domains in a ferroelectric state. The integration of the pyroelectric current provides a quantitative measure of the polarization change. However, special precautions have to be taken to ensure that the measured current actually reflects the polarization change and is free from artifacts such as electrical transport currents or capacitive contributions due to the sample's dielectric properties. The current measured in an experiment can be expressed by Eq. (1).

$$i = \frac{V}{R} + C\frac{dV}{dt} + \frac{dC}{dt}V + A\frac{dP}{dt}. \tag{1}$$

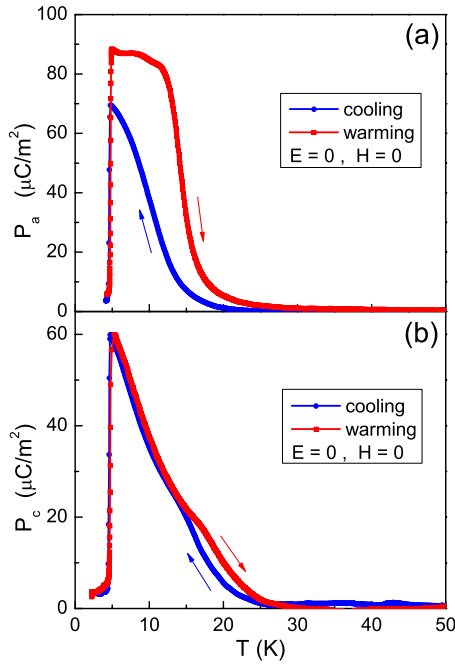V is the applied bias voltage, R and C are the resistance and capacitance of the sample, respectively, and P is the intrinsic

FIG. 6. (Color online) Polarization of $HoFe_3(BO_3)_4$ measured along (a): the a axis and (b): the c axis in zero electric and magnetic fields. The arrows distinguish the cooling and warming data.

electrical polarization. A is the contact area. The first term is the resistive current that can be avoided if the sample has a very high resistance or the measurement is conducted at zero bias, $V=0$. The effects of charge trapping and release with changing temperature usually are not significant for insulating materials. The second term is related to the charging current of a capacitor and will be zero if the applied voltage is constant with time. The third contribution in Eq. (1) may cause a current if the dielectric constant (capacitance) of the sample changes significantly with temperature (as for example ε_a in Fig. 5) and a bias voltage is applied. The resulting current can be estimated from the dielectric data and is negligible in most experiments. It can be avoided completely if no voltage bias is applied. The last term of Eq. (1) is the pyroelectric current due to the change of the sample's polarization. In the current experiments all polarization measurements have been conducted at zero-bias voltage, $V=0$, which ensures that the first three terms of Eq. (1) do not cause any additional contribution to the current so that the integration of the measured pyroelectric current yields the sample's polarization change. Measurements are commonly conducted by cooling the sample with an applied electrical bias voltage and measuring the pyroelectric current in zero bias upon warming.

In $HoFe_3(BO_3)_4$ we found that even in zero-voltage cooling the crystal developed a pyroelectric current arising below T_N at about 25 K. In passing through the spin reorientation transition the current shows a sharp negative peak indicating a sudden drop of the polarization. Integrating the current reveals the associated change of polarization shown in Fig. 6 [(a): a-axis and (b): c-axis polarization] for cooling and warming. Upon decreasing temperature, the polarizations measured along the a and c axes gradually increase in the

AFM2 phase and reach a maximum of 60 and 90 $\mu C/m^2$, respectively, at T_{SR}. A sharp drop of $P_{a,c}$ to a small value (presumably zero, the finite value shown in Fig. 6 is within the error limits of the measurement and integration) indicates the transition into the AFM1 phase. The maximum values of P_a and P_c are comparable with the magnitude of the polarization in the ferroelectric phase of other multiferroics, for example $Ni_3V_2O_8$ and $MnWO_4$.[31,32] However, there is a major difference in the temperature dependence of the polarization of $HoFe_3(BO_3)_4$ in comparison with the typical behavior observed in the majority of multiferroic ferroelectric compounds. In the latter compounds the ferroelectric polarization quickly increases below a magnetic phase transition and, in most cases, the direction of P is determined by the direction of the bias voltage applied during electric-field cooling. In the present data for $HoFe_3(BO_3)_4$ there is no significant change of $P(T)$ right below the magnetic transition temperature (38.5 K) but P_a and P_c smoothly increase below a much lower temperature ($\simeq 25$ K). Applying a poling voltage (± 150 V) had no sizable effect on $P(T)$ and the polarization could not be reversed. Pyroelectric current data measured upon cooling with a poling voltage applied as well as upon warming after the bias voltage was reduced to zero at 6 K are almost identical to the zero-bias data shown in Fig. 6. This indicates a strong preference of the direction of P_a and P_c which may be determined by structural or magnetic domains in contrast to most multiferroic ferroelectric systems. A clear thermal hysteresis of $P(T)$ between 15 and 25 K (indicated by arrows in Fig. 6) provides further evidence that the value of the polarization in the AFM2 phase is sensitive to the magnetic domain structure.

The most dramatic change of the dielectric constant ($\simeq 100\%$ increase, Fig. 5) was observed along the a axis. The maximum of the polarization $P_a(T)$ is also larger by about 50% than the maximum of P_c (Fig. 6) and the thermal hysteresis is even more significant and extends between T_{SR} and about 30 K. To investigate the effects of electric fields (bias voltage) on the polarization P_a the pyroelectric current was measured upon cooling to 6 K (above the spin reorientation transition) with a bias of ± 200 V applied. At 6 K the external voltage was set to zero and, after short circuiting the contacts, the remaining polarization was measured upon warming from 6 to 50 K. The data shown in Fig. 7 reveal a large apparent change of the polarization due to the external voltage. At $+200$ V cooling, $P_a(+200$ V) at 6 K is enhanced by 50% with respect to the zero-bias $P_a(0$ V) and at -200 V cooling, $P_a(-200$ V) is reduced to a fraction of less than 20%. The solid lines in Fig. 7 represent the polarization data obtained from integrating the pyroelectric current upon cooling in $+200$ V (top line), 0 V (center line), and -200 V (bottom line). After the release of the bias voltage at 6 K, however, the polarization assumes the zero-bias value close to 70 $\mu C/m^2$, as indicated by the vertical dotted arrows. Upon warming P_a follows closely the zero-bias temperature dependence (dashed lines in Fig. 7). The large change of P_a at 6 K upon release of the bias voltage seems to indicate a significant tunability of the polarization in electric fields.

However, the dielectric constant ε_a also increases significantly below T_N (Fig. 5) and the current contribution from the third term of Eq. (1) has to be taken into account in
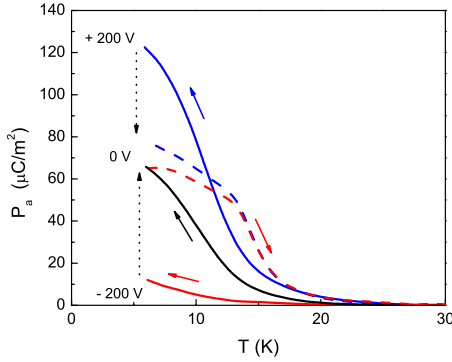
FIG. 7. (Color online) *a*-axis polarization of HoFe$_3$(BO$_3$)$_4$ measured upon cooling (solid lines) with applied bias voltage of +200, 0, and −200 V. Data upon warming (dashed lines) are collected after release of the bias voltage at 6 K.

measurements conducted in an external bias electric field to determine the intrinsic polarization values. From the dielectric measurements we determine the capacitance increase in the AFM2 phase as about 1 pF which results in an additional charge of $\pm 2 \times 10^{-10}$ C due to a bias voltage of ± 200 V. The change of the apparent polarization at 6 K in Fig. 7 (indicated by vertical dotted arrows) amounts to 2.2×10^{-10} and -2.7×10^{-10} C for a bias voltage of +200 and −200 V, respectively. After correcting for these additional contributions to the pyroelectric current, the values for P_a appear to change only very little in an electric field. Therefore, we conclude that for the *a*-axis pyroelectric measurement the zero-bias data (dashed lines in Fig. 7) are representative for the intrinsic polarization, $P_a(T)$. All subsequent pyroelectric measurements in magnetic fields have been conducted in zero electric field to avoid the additional contribution from the third term in Eq. (1) to the pyroelectric current measurement. It should be noted that this problem basically does not exist in the *c*-axis measurements [Fig. 6(a)] since the increase of ε_c in the AFM2 phase is negligibly small, only 3% of its value near T_N.

The appearance of a spontaneous polarization $P(T)$ in the AFM2 phase and its relative insensitivity to electric fields in HoFe$_3$(BO$_3$)$_4$ is unique among the rare earth iron borates. Changes of electrical polarization in RFe$_3$(BO$_3$)$_4$ have previously only been observed with the application and change of an external magnetic field for R=Gd (Ref. 2) and R=Nd.[6] The spontaneous polarization in HoFe$_3$(BO$_3$)$_4$ has its possible origin in the coupling to the internal magnetic field that is associated with the order of the iron spins as well as the Ho moments. It should be noted that a polarized state is not forbidden by the crystal symmetry because the P3$_1$21 space group is noncentrosymmetric. The magnetic order below T_N and its strong coupling to the lattice results in the development of a macroscopic electrical polarization. The preferred orientation of this polarization and the observation that it cannot be reversed by electric fields is a result of the noncentrosymmetric structure that allows for one direction of the polarization only within a structural and/or magnetic domain. Magnetic domains in the AFM2 phase, however, also play an important role as evidenced by the thermal hysteresis observed in the polarization data (Fig. 6) and it lends further

support to the role of the internal magnetic field/order and its mutual interaction with the polarization. From the measured polarization values along the *a* and *c* axes we conclude that the intrinsic polarization direction is between both major crystallographic orientations, at an angle of about 55° with the *c* axis. The origin of the intermediate orientation must be sought in the peculiarities of the magnetic structure. According to recent neutron scattering experiments[17] there exist two inequivalent Fe sites. In the polarized AFM2 phase the Fe(1)-spins and the Ho moments are aligned with the *a* axis, however, the spins on the Fe(2) sublattice are tilted toward the *c* axis. The estimated values of the *x* and *z* components of the Fe(2)-spins at 5 K are $4\mu_B$ and $2.5\mu_B$, respectively. The angle of the Fe(2)-spins with the *c* axis is therefore approximately 58°, close to the polarization orientation discussed above. While it seems unlikely that this coincidence is accidental it rather demonstrates the intricate coupling of the intrinsic polarization with the specifics of the magnetic order, supposedly of the Fe(2) sublattice.

The sharp drop of P_a and P_c at the spin reorientation transition indicates that the observed polarization is only allowed in the AFM2 phase with most of the magnetic moments oriented along the *a* axis (some iron spins have a *c* axis component, however).[17] In the low-temperature AFM1 phase all iron spins and half of the Ho moments are aligned with the *c* axis and the remaining Ho moments exhibit a tilt toward the *a* axis. The particular magnetic order apparently does not couple to the lattice to induce a macroscopic polarization. The microscopic details and the symmetry constraints have yet to be investigated. Forthcoming studies may also include the investigation of the dielectric relaxation behavior to gather complimentary knowledge about the nature of the polarized state.[33]

3. Magnetic-field effects on the polarization

To investigate the effects of external magnetic fields on the polarization, pyroelectric measurements have been conducted in zero electric field upon warming from the lowest temperatures (2 K) in a constant magnetic field H applied along the *a* and *c* axes. Results for the electrical polarization, P_c, are shown in Fig. 8. With H oriented along the *a* axis P_c is quickly diminished in even moderate magnetic fields [Fig. 8(a)]. The sharp drop of P_c to zero at T_{SR} persists up to the critical field above which the AFM1 phase is completely suppressed. At higher fields [10 kOe in Fig. 8(a)] P_c remains finite to the lowest temperatures although the overall magnitude is only about 15% of its maximum value at zero field. With the magnetic field applied along the *c* axis [Fig. 8(b)] the spin reorientation transition is quickly suppressed at low fields but the polarization retains its high values up to 8 kOe. At this field P_c remains large to the lowest temperatures. Only further increasing field reduces the magnitude of the polarization but at a lower rate as for the *a*-axis field. At 30 kOe the low-*T* polarization is still as large as 8 μC/m^2. The phase boundary separating the AFM2 and AFM1 phases as derived from the polarization drop (Fig. 8) is in perfect agreement with the phase diagrams shown in Fig. 3.

The polarization measured along the *a* axis, $P_a(T)$, is shown for different magnetic fields oriented along *a* and *c* in
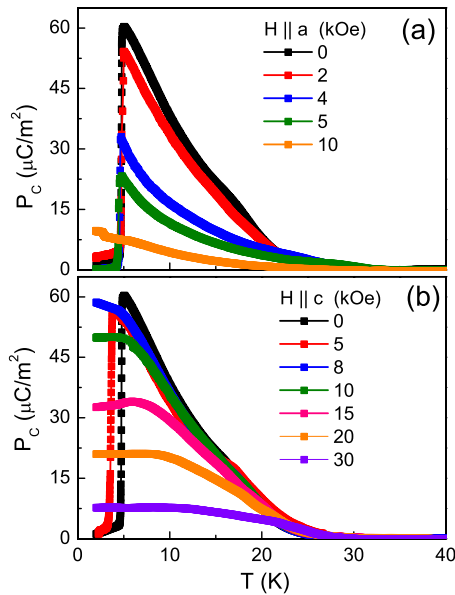
FIG. 8. (Color online) *c*-axis polarization of $HoFe_3(BO_3)_4$ at different magnetic fields *H*. (a): *H*∥*a* axis and (b): *H*∥*c* axis.

Fig. 9. $P_a(T)$ reveals a similar suppression in external magnetic fields as $P_c(T)$ discussed above. The *a*-axis magnetic field has the strongest effect on reducing P_a and even 2 kOe are sufficient to decrease P_a by 50%. The *c*-axis magnetic field suppresses the spin reorientation transition first while maintaining a relatively high magnitude of P_a up to about 10 kOe. Only higher fields H_c result in a slow decrease of P_a which reaches about 10% of the zero-field value at H_c =40 kOe. The hump of P_a that develops in magnetic fields between 15 and 20 K (Fig. 9) is associated with the temperature hysteresis in this range as shown in the zero-*H* polarization in Fig. 6. In magnetic fields the hysteretic region [extending from T_{SR} to about 25 K at *H*=0, Fig. 6(a)] shifts
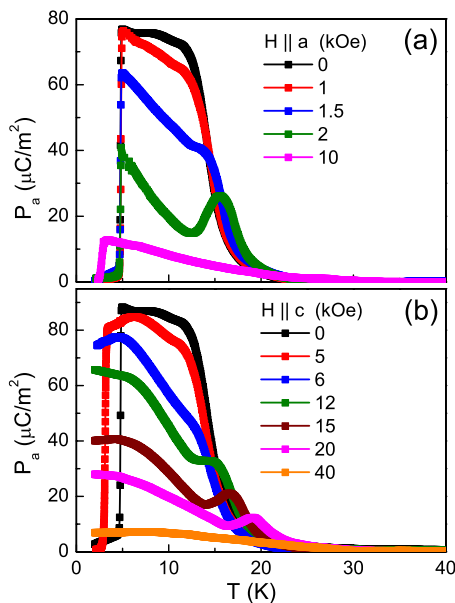

FIG. 9. (Color online) *a*-axis polarization of $HoFe_3(BO_3)_4$ at different magnetic fields *H*. (a): *H*∥*a* axis and (b): *H*∥*c* axis.
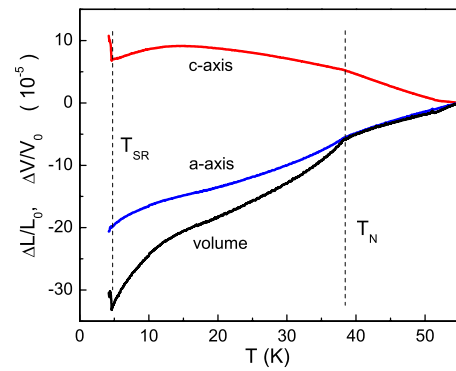

FIG. 10. (Color online) Thermal expansion of the *a* and *c* axes and the volume of $HoFe_3(BO_3)_4$. The two magnetic phase transitions are marked by vertical dashed lines.

toward higher temperature. For better clarity the polarization measured upon cooling is not included in Fig. 9. It seems surprising that the intrinsic zero-field polarization of $HoFe_3(BO_3)_4$ is quickly suppressed by external fields whereas in the related compound $NdFe_3(BO_3)_4$ the magnetic-field effect is significant and results in a large increase of the polarization. The major differences lie in the magnetic order of rare earth and iron moments below the Néel temperature. In $HoFe_3(BO_3)_4$ the spins on the Fe(1) sublattice are collinear (oriented along the *a* axis) with the Ho moments but noncollinear with the remaining spins on the Fe(2) sublattice.[17] In contrast, all Fe-spins in $NdFe_3(BO_3)_4$ are collinear with an easy-plane anisotropy and the Nd moments are noncollinear with the Fe spins.[19] These differences in the magnetic structures may be responsible for the different magnetoelectric properties.

4. Thermal expansion anomalies

The magnetoelectric coupling in multiferroic and magnetoelectric compounds are associated with ionic displacements at phase transitions that commonly result in macroscopic distortions or lattice strain along the crystallographic axes.[27,31,32,34,35] The relative change of the lattice parameters and the volume of $HoFe_3(BO_3)_4$ was therefore measured and is shown in Fig. 10. The reference temperature for both axes was chosen at 55 K. The dashed vertical lines indicate the two magnetic transitions. At T_N the temperature dependence of the *a* and *c* axes both exhibit a minute change of slope, as is expected for a second order magnetic phase transition. At T_{SR}, however, a sharp increase of *c* and the drop of *a* are characteristic for a first-order phase transition. The significant changes of the lattice parameters at T_{SR} are consistent with the abrupt disappearance of the electrical polarization and the sharp changes of the magnetic susceptibilities (Figs. 1 and 2). The large anomalies of the lattice parameters reveal the strong magnetoelastic effect in $HoFe_3(BO_3)_4$. It is interesting that the thermal expansivities are strongly anisotropic and the *c*-axis expansivity is negative over most of the temperature range shown in Fig. 10. Similar negative expansivities have been observed, for example, in multiferroic $HoMnO_3$ (Ref. 27) and $DyMn_2O_5$.[34] It was understood as a signature of strong magnetic correlations and spin-lattice in-
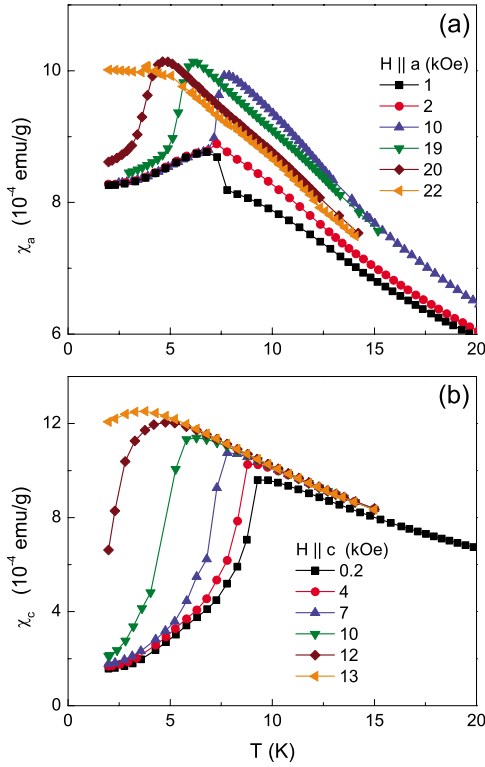
FIG. 11. (Color online) Magnetic susceptibility of $Ho_{0.5}Nd_{0.5}Fe_3(BO_3)_4$ at low temperatures in different magnetic fields. (a): $H\|a$ axis and (b): $H\|c$ axis.

teractions in connection with large magnetic anisotropy. The c-axis length exhibits a maximum at about 15 K. At lower temperatures both, c and a, decrease faster with decreasing temperature approaching the instability of the magnetic structure at the spin reorientation phase transition. The relative volume change (Fig. 10) clearly shows a rapid decrease below 15 K leading to the magnetic instability at $T_{SR}=4.6$ K.

C. Magnetic phase diagram, magnetoelectric effect, and polarization in $Ho_{0.5}Nd_{0.5}Fe_3(BO_3)_4$

$NdFe_3(BO_3)_4$ does not show any evidence for a spin reorientation phase transition at low temperatures[19,23] but it exhibits a large magnetoelectric effect.[6] The solid solution of $NdFe_3(BO_3)_4$ and $HoFe_3(BO_3)_4$ is therefore of interest with regard to the magnetic phase diagram and the magnetoelectric properties.

1. Magnetic phase diagram

The magnetic susceptibility was measured in $Ho_{0.5}Nd_{0.5}Fe_3(BO_3)_4$ for both field orientations, H_a and H_c. χ_a and χ_c show a sizable steplike change at $T_{SR}\simeq9$ K, clearly revealing the existence of a spin reorientation transition. While the drop of χ_c at T_{SR} is large in passing into the AFM1 phase and it amounts up to 80%, the change of χ_a is moderate and less than 20%, similar to $HoFe_3(BO_3)_4$. However, the anomaly of χ_a changes sign at about 2 kOe. Below 2 kOe, upon decreasing temperature, the step of χ_a is posi-
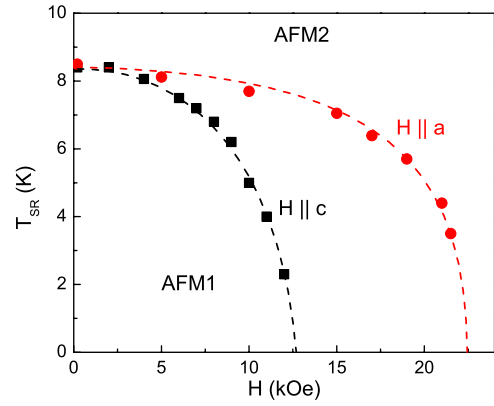

FIG. 12. (Color online) Low-temperature magnetic phase diagram of $Ho_{0.5}Nd_{0.5}Fe_3(BO_3)_4$.

tive whereas above 2 kOe it is negative. At 2 kOe the anomaly of χ_a at T_{SR} is a change of slope with no sudden change, as shown in Fig. 11(a). A similar behavior is also observed in the polarization P_a in magnetic fields applied along the a axis (next section). It is remarkable that T_{SR} of $Ho_{0.5}Nd_{0.5}Fe_3(BO_3)_4$ is twice as large as that of $HoFe_3(BO_3)_4$. However, it is comparable with T_{SR} of $GdFe_3(BO_3)_4$.[5] The larger value of T_{SR} indicates that Nd stabilizes the low-temperature AFM1 phase and T_{SR} passes through a maximum in the phase diagram of the solid solution $Ho_{1-x}Nd_xFe_3(BO_3)_4$. The AFM1 phase in $Ho_{0.5}Nd_{0.5}Fe_3(BO_3)_4$ is also more stable with respect to magnetic fields as compared to $HoFe_3(BO_3)_4$. The magnetic phase diagram derived from a- and c-axis magnetization measurements is shown in Fig. 12. The phase diagram includes data of $\chi(T)$ acquired upon cooling and warming and results from isothermal magnetization measurements with increasing and decreasing fields. In comparison to $HoFe_3(BO_3)_4$ the AFM1 phase of $Ho_{0.5}Nd_{0.5}Fe_3(BO_3)_4$ is more stable with respect to temperature as well as magnetic field. The zero-temperature critical fields of the AFM1 $\rightarrow$ AFM2 transition are estimated as 22 and 13 kOe for $H\|a$ and $H\|c$, respectively.

The thermodynamic signatures of both magnetic phase transitions, paramagnetic $\rightarrow$ AFM2 and AFM2 $\rightarrow$ AFM1, are resolved in distinct anomalies of the heat capacity shown in Fig. 13. The λ-shaped peak at $T_N=32$ K is characteristic for a second-order phase transition. The first-order spin reorientation transition is clearly marked by the sharp peak at about 9 K. While the peak at T_{SR} appears on top of a broad shoulder there is no clear maximum of C_p/T at lower temperatures that could indicate a Schottky type anomaly as observed for example in $NdFe_3(BO_3)_4$ [23] or $GdFe_3(BO_3)_4$ (Fig. 4). The major difference to $HoFe_3(BO_3)_4$ discussed above is the significantly lower Neél temperature of the iron spin order and the larger spin reorientation temperature.

2. Magnetoelectric properties of $Ho_{0.5}Nd_{0.5}Fe_3(BO_3)_4$

At zero magnetic field the spontaneous polarization measured along the a axis, $P_a(T)$, arises below 40 K in $Ho_{0.5}Nd_{0.5}Fe_3(BO_3)_4$ and it reaches a maximum at the spin reorientation transition (Fig. 14). The maximum value of
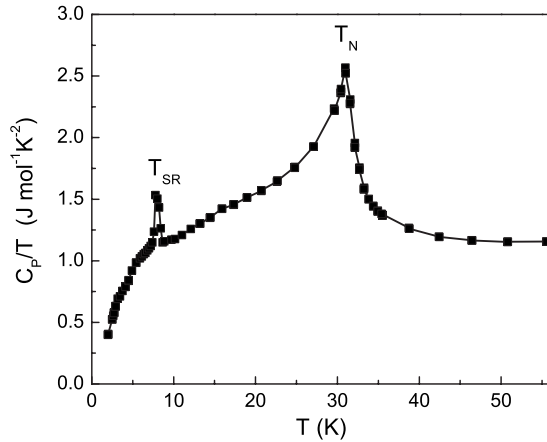
FIG. 13. Heat capacity of $Ho_{0.5}Nd_{0.5}Fe_3(BO_3)_4$.

$120 \ \mu C/m^2$ exceeds the corresponding value of $HoFe_3(BO_3)_4$ by a factor of 2. The transition into the AFM1 phase is accompanied by a sharp drop of P_a, however, P_a remains finite (about $40 \ \mu C/m^2$) in the low-temperature AFM1 phase. This is in distinct contrast to the behavior in $HoFe_3(BO_3)_4$ (Fig. 9), where P_a drops to zero in the AFM1 phase. With the external magnetic field applied along the c axis [Fig. 14(b)], the spin reorientation transition temperature is reduced resulting in an enhancement of the maximum of $P_a(T)$ to $160 \ \mu C/m^2$ for fields up to 20 kOe. At higher magnetic fields H_c the polarization decreases continuously over the whole temperature range and its maximum value drops to $20 \ \mu C/m^2$ at $H_c = 7$ T.

The magnetic-field dependence of P_a of $Ho_{0.5}Nd_{0.5}Fe_3(BO_3)_4$ for $H \| c$ is qualitatively similar to the
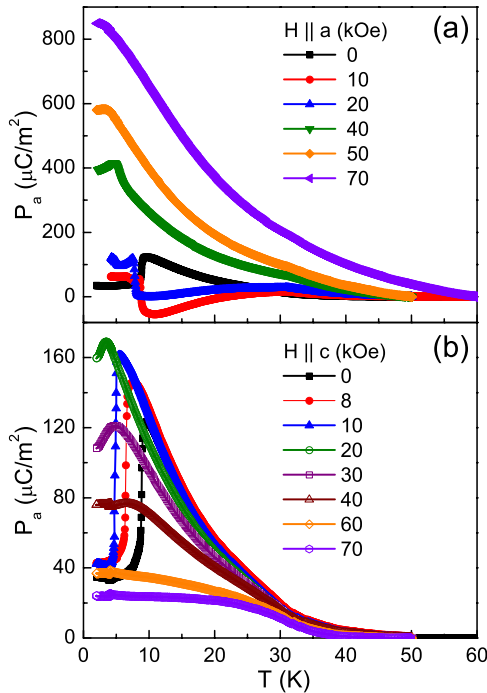
FIG. 14. (Color online) Temperature dependence of $P_a(T)$ of $Ho_{0.5}Nd_{0.5}Fe_3(BO_3)_4$ in different magnetic fields, (a): $H \| a$ axis and (b): $H \| c$ axis.
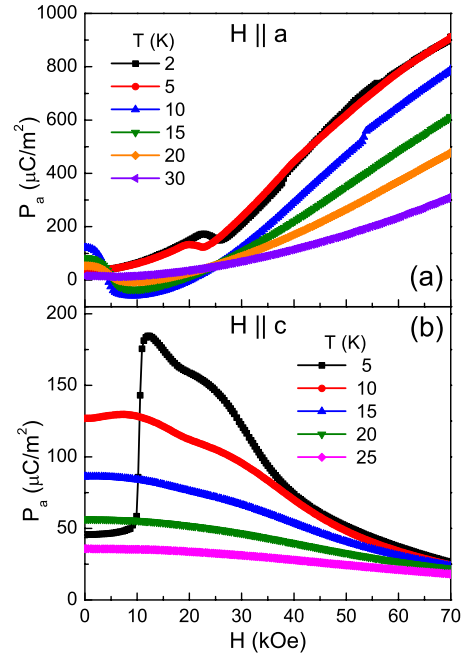
FIG. 15. (Color online) Magnetic-field dependence of the polarization P_a at different temperatures. (a): $H \| a$ axis and (b): $H \| c$ axis

field effect in $HoFe_3(BO_3)_4$ as is also obvious from the isothermal polarization measurements shown in Fig. 15(b). The polarization $P_a(H_c)$ of Fig. 15 was derived from current measurements at constant temperature and increasing field. The value of P_a at zero field was determined from the T-dependent data (Fig. 14) at $H_c = 0$ as the reference value. At 5 K the polarization P_a is finite and nearly constant for small fields but it increases sharply at 10 kOe because of the transition from the AFM1 to the AFM2 phase. With further increasing field $P_a(5 \text{ K})$ decreases quickly, consistent with the T-dependent data of Fig. 14(b). At higher temperatures (>10 K)P_a starts higher at zero field because of its larger value in the AFM2 phase. However, the external magnetic field H_c reduces P_a quickly as shown in Fig. 15(b). The critical temperatures and fields of the spin reorientation phase transition determined by the sharp change of the polarization [Figs. 14(b) and 15(b)] coincide with the c-axis magnetic phase diagram of Fig. 12 derived from magnetization measurements.

The effect of the c-axis magnetic field on the polarization of $Ho_{0.5}Nd_{0.5}Fe_3(BO_3)_4$ is similar to the field-induced suppression of the spontaneous polarization of $HoFe_3(BO_3)_4$. However, the picture changes completely if the magnetic field is applied along the hexagonal a axis. The polarization $P_a(T)$ at various H_a is shown in Fig. 14(a). In zero magnetic field $P_a(T)$ arises below T_N, exhibits the maximum at T_{SR} and drops sharply to a smaller value in the AFM1 phase, as discussed above. With increasing magnetic field, however, the positive $P_a(T)$ is suppressed, it becomes negative, and passes through a minimum with decreasing temperature, as shown in Fig. 14(a) for $H_a = 10$ kOe. The sudden decrease of $P_a(H=0)$ at T_{SR} is inverted in fields above 2 kOe and P_a increases sharply with the transition into the AFM1 phase. This behavior of P_a at T_{SR} is consistent with the anomaly of

the magnetization discussed in the previous section demonstrating the close relation of the spontaneous polarization and the magnetization.

With the magnetic field increasing further above 10 kOe the polarization $P_a(T)$ starts increasing again in the whole temperature range even above the AFM Néel temperature. P_a is all positive for $H_a > 20$ kOe and it increases to large values, $P_a > 800$ $\mu C/m^2$, at 70 kOe and 2 K (Fig. 14(a)). This high-field behavior is similar to the magnetoelectric effect observed in NdFe$_3$(BO$_3$)$_4$ and can be attributed to a quadratic magnetoelectric coupling as discussed recently.[6]

The complex temperature and field dependence of $P_a(T)$ shown in Fig. 14(a) is also reflected in the isothermal polarization data, $P_a(H_a)$. The results at different temperatures are displayed in Fig. 15(a). At zero and small field P_a is positive and determined by the spontaneous polarization as discussed above. With increasing field the spontaneous P_a is suppressed, similar to the effect of a c-axis field [Figs. 14(a) and 15(a)] and the field effect in HoFe$_3$(BO$_3$)$_4$ (Sec. III B). The magnetoelectric effect, since quadratic in H_a,[6] is negligibly small. The steplike anomaly of P_a near 22 kOe [2 and 5 K data of Fig. 15(a)] is consistent with the temperature anomaly of P_a at T_{SR} [Fig. 14(a)]. However, at higher field the magnetoelectric coupling dominates, similar to NdFe$_3$(BO$_3$)$_4$. The magnetoelectric effect at first decreases the polarization and $P_a(H_a)$ changes sign and becomes negative above about 4 kOe. With further increasing H_a the magnetoelectric effect changes sign and results in another sign reversal of $P_a(H_a)$ at about 20 kOe. This effect was also observed in NdFe$_3$(BO$_3$)$_4$ and it was explained by the competition of the external magnetic field with the exchange field.[6] The major difference of the polarization behavior of NdFe$_3$(BO$_3$)$_4$ and Ho$_{0.5}$Nd$_{0.5}$Fe$_3$(BO$_3$)$_4$ is the existence of a polarization P_a in zero magnetic field which is aligned with the high-field magnetoelectric polarization. The spontaneous polarization and the field induced magnetoelectric polarization are superimposed and result in a twofold sign reversal of the total polarization upon increasing external magnetic field between 10 and 20 K, as shown in Fig. 15(a).

We have also conducted pyroelectric measurements along the hexagonal c axis. The detected pyroelectric current was very small and any possible component of the polarization in zero and high magnetic fields was beyond the resolution limits of the experimental procedure.

IV. SUMMARY AND CONCLUSIONS

We have investigated the thermodynamic, magnetic, dielectric, and magnetoelectric properties of HoFe$_3$(BO$_3$)$_4$ and Ho$_{0.5}$Nd$_{0.5}$Fe$_3$(BO$_3$)$_4$. Both compounds show an antiferromagnetic Néel transition at $T_N = 38.5$ K (HoFe$_3$(BO$_3$)$_4$) and $T_N = 32$ K [Ho$_{0.5}$Nd$_{0.5}$Fe$_3$(BO$_3$)$_4$] into the AFM2 phase and a spin reorientation phase transition at T_{SR} into a low-temperature AFM1 phase. The AFM1 phase is suppressed in external magnetic fields oriented along the a and c axes. The thermodynamic signature of both magnetic transitions is shown in distinct anomalies of the heat capacity indicating a second order transition at T_N and a first-order phase transition at T_{SR}. The magnetic phase diagram of both compounds is completely resolved up to 70 kOe.

The dielectric and magnetoelectric experiments on HoFe$_3$(BO$_3$)$_4$ reveal giant magnetodielectric effect and the existence of a spontaneous polarization below the Néel temperature which suddenly drops to zero at T_{SR}. This effect has not been observed before in rare earth iron borates. The polarization in HoFe$_3$(BO$_3$)$_4$ has components along the a and c axes indicating its internal orientation in between both crystallographic orientations. This polarization only arises in the AFM2 phase of HoFe$_3$(BO$_3$)$_4$ which shows that P is tied to the magnetic order and the resulting internal magnetic field of this phase. In contrast to NdFe$_3$(BO$_3$)$_4$ external magnetic fields do mainly suppress the polarization and the magnetoelectric effect is negative, $dP/dH < 0$. A symmetry analysis similar to NdFe$_3$(BO$_3$)$_4$ (Ref. 6) may help to clarify the origin of the zero-field polarization of HoFe$_3$(BO$_3$)$_4$. This analysis has to take into account the specific magnetic order of both, Fe and Ho subsystems, as known from neutron scattering data.[17]

Substituting 50% of Ho with Nd results in a reduction of T_N to 32 K and an increase of the stability range of the AFM1 phase. The spontaneous polarization at zero magnetic field is also observed, mainly along the a axis, with an increase of the maximum polarization (at zero magnetic field) by 50% as compared to the values in HoFe$_3$(BO$_3$)$_4$. Similar to HoFe$_3$(BO$_3$)$_4$, magnetic fields along the c axis suppress the polarization of Ho$_{0.5}$Nd$_{0.5}$Fe$_3$(BO$_3$)$_4$. However, the a-axis magnetic field couples to the polarization and the magnetoelectric effect induces large values of the polarization P_a (up to 900 $\mu C/m^2$ at 70 kOe). The temperature and field dependence of P_a is very complex with several sign reversals of the polarization and steplike anomalies at the spin reorientation phase transition. The detailed features can be understood as a superposition of the spontaneous polarization induced by internal fields and the magnetoelectric effect due to the external magnetic field. The solid solution Ho$_{0.5}$Nd$_{0.5}$Fe$_3$(BO$_3$)$_4$ combines features observed in both parent compounds, HoFe$_3$(BO$_3$)$_4$ and NdFe$_3$(BO$_3$)$_4$.

Further investigations of the magnetic structure, the order of Fe spins, Ho and Nd moments, and the magnetoelectric interactions are necessary to gather a basic understanding of the complex physical properties of Ho$_{0.5}$Nd$_{0.5}$Fe$_3$(BO$_3$)$_4$ and related compounds. The present investigation may be extended to include the solid solution of other members of the rare earth iron borate compounds. One interesting candidate could be the solid solution of Ho$_{1-x}$Gd$_x$Fe$_3$(BO$_3$)$_4$. GdFe$_3$(BO$_3$)$_4$ is the only second compound in the rare earth iron borate system to show a significant magnetoelectric effect and, therefore, the magnetoelectric properties of Ho$_{1-x}$Gd$_x$Fe$_3$(BO$_3$)$_4$ should be interesting too. A thorough investigation of Ho$_{1-x}$Gd$_x$Fe$_3$(BO$_3$)$_4$ could even help to arrive at a deeper and more comprehensive understanding of the current results on Ho$_{0.5}$Nd$_{0.5}$Fe$_3$(BO$_3$)$_4$.

[1] J.-C. Joubert, W. B. White, and R. Roy, J. Appl. Crystallogr. **1**, 318 (1968).

[2] A. K. Zvezdin, S. S. Krotov, A. M. Kadomtseva, G. P. Vorb'ev, Y. F. Popov, A. P. Pyatakov, L. N. Bezmaternykh, and E. A. Popova, JETP Lett. **81**, 272 (2005).

[3] S. S. Krotov, A. M. Kadomtseva, Y. F. Popov, G. P. Vorob'ev, A. V. Kuvardin, K. I. Kamilov, L. N. Bezmaternykh, and E. A. Popova, J. Magn. Magn. Mater. **300**, e426 (2006).

[4] A. K. Zvezdin, A. M. Kadomtseva, S. S. Krotov, A. P. Pyatakov, Y. F. Popov, and G. P. Vorob'ev, J. Magn. Magn. Mater. **300**, 224 (2006).

[5] F. Yen, B. Lorenz, Y. Y. Sun, C. W. Chu, L. N. Bezmaternykh, and A. N. Vasiliev, Phys. Rev. B **73**, 054435 (2006).

[6] A. K. Zvezdin, G. P. Vorob'ev, A. M. Kadomtseva, Y. F. Popov, A. P. Pyatakov, L. N. Bezmaternykh, A. V. Kuvardin, and E. A. Popova, JETP Lett. **83**, 509 (2006).

[7] A. M. Kalashnikova, V. V. Pavlov, R. V. Pisarev, L. N. Bezmaternykh, M. Bayer, and T. Rasing, JETP Lett. **80**, 293 (2004).

[8] A. G. Gavriliuk, S. A. Kharlamova, I. S. Lyubutin, I. A. Troyan, S. G. Ovchinnikov, A. M. Potseluiko, M. I. Eremets, and R. Boehler, JETP Lett. **80**, 426 (2004).

[9] Ph. Goldner, O. Guillot-Noël, J. Petit, M. Popova, and L. Bezmaternykh, Phys. Rev. B **76**, 165102 (2007).

[10] S. Klimin, D. Fausti, A. Meetsma, L. N. Bezmaternykh, P. H. M. van Loosdrecht, and T. T. M. Palstra, Acta Crystallogr. B **61**, 481 (2005).

[11] D. Fausti, A. A. Nugroho, P. H. M. van Loosdrecht, S. A. Klimin, M. N. Popova, and L. N. Bezmaternykh, Phys. Rev. B **74**, 024403 (2006).

[12] Y. Hinatsu, Y. Doi, K. Ito, M. Wakeshima, and A. Alemi, J. Solid State Chem. **172**, 438 (2003).

[13] A. N. Vasiliev, E. A. Popova, I. A. Gugim, L. N. Bezmaternykh, and Z. Hiroi, J. Magn. Magn. Mater. **300**, e382 (2006).

[14] A. D. Balaev, L. N. Bezmaternykh, I. A. Gudim, V. L. Temerov, S. G. Ovchinnikov, and S. A. Kharlamova, J. Magn. Magn. Mater. **258-259**, 532 (2003).

[15] R. Z. Levitin, E. A. Popova, R. M. Chtsherbov, A. N. Vasiliev, M. N. Popova, E. P. Chukalina, S. A. Klimin, P. H. M. van Loosdrecht, D. Fausti, and L. N. Bezmaternykh, JETP Lett. **79**, 423 (2004).

[16] A. I. Pankrats, G. A. Petrakovskii, L. N. Bezmaternykh, and O. A. Bayukov, Sov. Phys. JETP **99**, 766 (2004).

[17] C. Ritter, A. Vorontynov, A. Pankrats, G. Petrakovskii, V. Temerov, I. Gudim, and R. Szymczak, J. Phys.: Condens. Matter **20**, 365209 (2008).

[18] H. Mo, C. S. Nelson, L. N. Bezmaternykh, and V. T. Temerov, Phys. Rev. B **78**, 214407 (2008).

[19] P. Fischer, V. Pomjakushin, D. Sheptyakov, L. Keller, M. Janoschek, B. Roessli, J. Schefer, G. Petrakovskii, L. Bezmaternykh, V. Temerov, and D. Velikanov, J. Phys.: Condens. Matter **18**, 7975 (2006).

[20] C. Ritter, A. Balaev, A. Vorontynov, G. Petrakovskii, D. Velikanov, V. Temerov, and I. Gudim, J. Phys.: Condens. Matter **19**, 196227 (2007).

[21] A. M. Kadomtseva, A. K. Zvezdin, A. P. Pyatakov, A. V. Kuvardin, G. P. Vorob'ev, Y. F. Popov, and L. N. Bezmaternykh, Sov. Phys. JETP **105**, 116 (2007).

[22] A. M. Kadomtseva, Y. F. Popov, S. S. Krotov, G. P. Vorob'ev, E. A. Popova, A. K. Zvezdin, and L. N. Bezmaternykh, Low Temp. Phys. **31**, 807 (2005).

[23] N. Tristan, R. Klingeler, C. Hess, B. Büchner, E. Popova, I. A. Gudim, and L. N. Bezmaternykh, J. Magn. Magn. Mater. **316**, e621 (2007).

[24] M. N. Popova, E. P. Chukalina, T. N. Stanislavchuk, B. Z. Malkin, A. R. Zakirov, E. Antic-Fidancev, E. A. Popova, L. N. Bezmaternykh, and V. L. Temerov, Phys. Rev. B **75**, 224435 (2007).

[25] J. A. Campá, C. Cascales, E. Gutiérrez-Puebla, M. A. Monge, I. Rasines, and C. Ruíz-Valero, Chem. Mater. **9**, 237 (1997).

[26] L. N. Bezmaternykh, V. L. Temerov, I. A. Gudim, and N. A. Stolbovaya, Crystallogr. Rep. **50**, S97 (2005).

[27] C. R. dela Cruz, F. Yen, B. Lorenz, Y. Q. Wang, Y. Y. Sun, M. M. Gospodinov, and C. W. Chu, Phys. Rev. B **71**, 060407(R) (2005).

[28] T. N. Stanislavchuk, E. P. Chukalina, M. N. Popova, L. N. Bezmaternykh, and I. A. Gudim, Phys. Lett. A **368**, 408 (2007).

[29] B. Lorenz, Y. Q. Wang, Y. Y. Sun, and C. W. Chu, Phys. Rev. B **70**, 212412 (2004).

[30] B. Lorenz, Y.-Q. Wang, and C.-W. Chu, Phys. Rev. B **76**, 104405 (2007).

[31] R. P. Chaudhury, F. Yen, C. R. dela Cruz, B. Lorenz, Y. Q. Wang, Y. Y. Sun, and C. W. Chu, Phys. Rev. B **75**, 012407 (2007).

[32] R. P. Chaudhury, F. Yen, C. R. dela Cruz, B. Lorenz, Y. Q. Wang, Y. Y. Sun, and C. W. Chu, Physica B **403**, 1428 (2008).

[33] F. Schrettle, P. Lunkenheimer, J. Hemberger, V. Yu. Ivanov, A. A. Mukhin, A. M. Balbashov, and A. Loidl, Phys. Rev. Lett. **102**, 207208 (2009).

[34] C. R. dela Cruz, F. Yen, B. Lorenz, M. M. Gospodinov, C. W. Chu, W. Ratcliff, J. W. Lynn, S. Park, and S.-W. Cheong, Phys. Rev. B **73**, 100406(R) (2006).

[35] C. R. dela Cruz, B. Lorenz, Y. Y. Sun, C. W. Chu, S. Park, and S.-W. Cheong, Phys. Rev. B **74**, 180402(R) (2006).